An Effective Water Depth Correction for Pressure-Based Wave Statistics on Rough Bathymetry

Olavo B. Marques,[a, b] Falk Feddersen,[a] James MacMahan,[b]

[a] *Scripps Institution of Oceanography, University of California, San Diego, La Jolla, California*

[b] *Oceanography Department, Naval Postgraduate School, Monterey, California*

Corresponding author: Olavo B. Marques, omarques@ucsd.edu

ABSTRACT: Near-bottom pressure sensors are widely used to measure surface gravity waves. Pressure spectra are usually converted to sea surface elevation spectra with a linear-theory transfer function assuming constant depth. This methodology has been validated over smooth sandy beaches, but not over complex bathymetry of coral reefs or rocky coasts. Bottom-mounted pressure sensors co-located with wave buoys in 10–13 m water depth from a 5-week rocky-shorelines experiment are used to quantify the error of pressure-based surface gravity wave statistics and develop correction methods. The rough bathymetry has $O(1)$ m vertical variability on $O(1-10)$ m horizontal scales, much shorter than the 90–40 m wavelength of sea-band (0.1-0.2 Hz). For sensor stability, pressure sensors were deployed by divers in bathymetric lows. An effective depth hypothesis is proposed where a spatially smoothed water depth provides more accurate wave height statistics than the local depth at the pressure sensor. Pressure-based significant wave height squared overestimates (as large as 21%) the direct wave buoy measurements, with elevated biases in sea band, when using the pressure-sensor water depth in a bathymetric low. An optimal depth correction, estimated by minimizing the wave height error, varies from 0.1–1.6 m. A bathymetry smoothing scale of 13 m (1/3 of wavelength at 0.2 Hz) is found by minimizing the smoothed bathymetry deviation relative to the optimal. The optimal and smoothed bathymetry depth corrections are similar across locations and both corrections, using linear theory, significantly reduce wave statistical errors. This suggests pressure sensor measurements can be effectively corrected in regions with strong bathymetric variability over short length scales.

SIGNIFICANCE STATEMENT: The measurement of surface waves by bottom-mounted pressure sensors relies on wave theory formally derived for constant depth. We show that the constant depth assumption leads to systematic errors in wave statistics from observations over a rough, rocky bottom. By considering a spatially-smoothed bathymetry instead of the local water depth at the pressure sensor, the accuracy of wave energy density can be improved from 20% to 10%.

1. Introduction

Pressure sensors are routinely used to describe surface gravity wave statistics such as wave spectra, significant wave height, and wave energy flux, and are fundamental to observations of wave transformation in the nearshore. Cross-shore arrays of pressure sensors provide gradients in sea-swell wave statistics associated with wave shoaling and dissipation on sandy shore environments (e.g., Thornton and Guza 1982, 1983; Raubenheimer et al. 1996; Herbers et al. 1999), coral reef environments (e.g., Lowe et al. 2005; Monismith et al. 2015; Lentz et al. 2016; Rogers et al. 2016; Acevedo-Ramirez et al. 2021; Sous et al. 2023), and rocky shores (Farrell et al. 2009; Poate et al. 2018; Gon et al. 2020; Lavaud et al. 2022). The energetics of surface gravity waves are important for driving several processes in the nearshore, such as the circulation (e.g., MacMahan et al. 2006), infragravity waves (e.g., Bertin et al. 2018), runup at the shoreline (e.g., Gomes da Silva et al. 2020), sediment transport on sandy beaches (e.g., Elfrink and Baldock 2002), and dispersal of tracers (e.g., Moulton et al. 2023). Accurate estimates of surface gravity wave statistics from pressure sensors are crucial for measuring how waves transform, drive currents, and induce mixing between the surfzone and inner shelf.

Surface gravity wave statistics are typically estimated from pressure measurements using linear wave theory and assuming constant water depth, h. A transfer function K converts the observed pressure spectrum ($S_p(f)$, where f is frequency) to a surface elevation spectrum ($S_\eta(f)$), i.e.,

$$S_\eta(f) = K^2 S_p(f), \tag{1}$$

where K is given by (e.g., Dean and Dalrymple 1991)

$$K = \frac{\cosh(kh)}{\cosh(kz_{\mathrm{hab}})}, \tag{2}$$

where z_{hab} is the height above the bottom for the pressure measurement, and k is the radian wavenumber derived from the linear-theory dispersion relationship,

$$\omega^2 = gk \tanh(kh), \tag{3}$$

where ω is the radian wave frequency ($\omega = 2\pi f$) and g is the gravitational acceleration. In practice, the water depth h is estimated from the mean pressure and knowing z_{hab}. In many nearshore applications, pressure sensors are deployed near the bed. Thus, z_{hab} is often small (1-10 cm) and $\cosh(kz_{\text{hab}}) \approx 1$. Similar transfer functions can be derived for constant depth from linear theory to relate horizontal and vertical velocity spectra to S_η (Herbers et al. 1992).

A well-known issue with this transformation is that K grows exponentially at large kh so that pressure noise becomes amplified, and typically a high-frequency cut-off is applied to avoid contamination of wave statistics (e.g., Raubenheimer et al. 1996). Validation of pressure-based wave height statistics from (1)-(3) against statistics from direct measurements of the surface elevation in the laboratory (Bishop and Donelan 1987) and in the field (Guza and Thornton 1980) reported an accuracy within 10%, where the validation was performed over $0.1 < kh < 2$, with small enough K^2 to prevent noise amplification. A few comparisons have been obtained between directly measured $S_\eta(f)$ and $K^2 S_p$ on the inner shelf. In a low-sloped sandy bay, co-located Spotter (GPS-based) wave buoy and pressure sensor integrated within an ADCP (Acoustic Doppler Current Profiler) in $h \approx 7$ m have a good time-mean spectral comparison in the sea-swell (0.05–0.2 Hz) band (Lancaster et al. 2021). Offshore of a low-sloped sandy beach in $h \approx 10$ m, a comparison between a pressure sensor and an acoustic surface tracker on an ADCP showed that linear theory accurately estimated S_η out to at least $kh \approx 1.5$ (Martins et al. 2021). Recently a comparison of various wave buoys and a pressure sensor array in 8-m water depth, showed that the wave buoys were consistent with the linear-theory transformed pressure measurements across the 0.07–0.25 Hz band (Collins et al. 2023). The linear-theory transfer function (2) is derived under a constant h approximation. For smooth and weak bathymetric slope (i.e., bathymetry varying on scales longer than a wavelength), this assumption works well both seaward of the surfzone (e.g., Herbers et al. 1992; Collins et al. 2023) where bathymetric slopes are typically < 0.01 and through the surfzone (e.g., Thornton and Guza 1983; Herbers et al. 1999) where bathymetric slopes are generally < 0.04.

Wave nonlinearity is not incorporated in (1)-(3), and increasingly nonlinear waves modify the relationship between near-bed pressure and sea-surface elevation. A weakly nonlinear and weakly dispersive (small kh) method can reproduce the sea-surface of a soliton from bottom pressure (Bonneton and Lannes 2017) and wave time series for just offshore of the surfzone (Bonneton et al. 2018). For $O(1)$ kh where triads are not resonant, the relationship between S_η and S_p can change as a certain fraction of the wave energy at a particular frequency is bound (e.g., Hasselmann 1962). However, in ≈ 7 m depth, the fraction of bound energy at $f < 0.2$ Hz is generally small even for large waves (Herbers et al. 1992), and the relationship between pressure and velocity is well predicted by linear wave theory (Herbers et al. 1992). This relationship is so consistent even within the surfzone that it is used as a method of quality controlling current meter data (Elgar et al. 2001). For weakly dispersive waves, large waves can also change the dispersion relationship through amplitude dispersion which was detectable in the field (Herbers et al. 2002) and laboratory (Martins et al. 2021).

Linear theory also neglects the velocity-squared terms in the Bernoulli equation, which can be significant for estimating wave setdown and setup (Raubenheimer et al. 2001). However, for realistic conditions, this term contributes 2.5 cm root-mean-square to hydrostatic pressure (Lentz and Raubenheimer 1999) and is thus generally negligible for estimating wave properties.

In contrast with sandy beaches, coral reefs and rocky shores support large multiscale bathymetric variability at scales much shorter than the sea-swell wavelengths (i.e., large slopes and slope variability), and the constant h assumption in (1)-(3) is questionable. For example, coral reef bathymetry has steep fore reefs, gently sloping flat reefs, and spur-and-groove formations, all of which can have $O(1)$ m depth changes over $O(1)$ m horizontal distance (e.g., Monismith 2007; Davis et al. 2021), scales much shorter than the $O(10-100)$ m wavelength of sea-swell waves. Despite complex bathymetry, wave statistics are often estimated by applying linear wave theory to pressure sensor data, taking h as the depth calculated from the data (e.g., Monismith et al. 2015). Similarly, wave height estimates from pressure sensors have also been made over rocky bathymetry, which may have $O(1)$ m variability in h over horizontal scales much shorter than sea-swell wavelengths (Farrell et al. 2009; Poate et al. 2018; Gon et al. 2020; Lavaud et al. 2022). No validation of pressure-derived wave statistics has been performed on coral reefs or rocky shores.

Assuming a constant h approximation with (2)-(3) can be used in rough complex bathymetric regions to derive wave statistics, it is unclear that the local pressure-sensor estimated h is the appropriate choice. For wavelengths and water depths with small kh (e.g., Lentz et al. 2016), waves are largely hydrostatic, K is approximately 1 throughout the water column, and the choice of h may not be important. However, in regions with $O(1)$ kh and rough bathymetry, the transfer function is likely sensitive to the depth, which would affect wave statistics. Accurate surface gravity wave statistics are particularly important for spatial instrument arrays where gradients of wave statistics are taken across horizontal scales of $O(10-100)$ m. Gradients of wave energy flux derived from pressure sensors show larger wave bottom friction dissipation over coral reefs or rocky shores than on sandy beaches (e.g., Lowe et al. 2005; Gon et al. 2020). Large bottom friction dissipation has been observed (Lowe et al. 2005; Gon et al. 2020) at large water depth, where depth-limited wave breaking is negligible, but errors in K for large kh could be significant. Therefore, if the constant depth assumption underlying (1)-(3) lead to substantial errors in the surface elevation spectrum, the contamination not only extends to wave height and energy flux but also to wave dissipation estimates across the array.

Here we use bottom-mounted pressure sensors with co-located wave buoys to address the accuracy of linear wave theory to estimate wave heights from pressure data over complex and rough bathymetry in approximately 10 m water depth. Observations are from a 5-week experiment that was carried out in the Monterey Peninsula (California, USA) as part of ROXSI (ROcky Shore: eXperiment and SImulations). The instrument array and bathymetry are described in Section 2. The accuracy of (1)-(3) with a local water depth is quantified in Section 3. In Section 4, we propose and test an effective depth hypothesis, where the depth from a spatially-smoothed bathymetry results in more accurate wave statistics than the local depth from a pressure sensor. Comparisons with a sandy inner-shelf, the implications of the effective depth, and application to coral reefs are discussed in Section 5. A summary is presented in Section 6.

2. Methods

a. Field site and bathymetry

The first ROXSI (ROcky shores: eXperiments and SImulations) field experiment was carried out off China Rock, Pebble Beach, CA, USA during June-July 2022 (Fig. 1). The goal of ROXSI is to study how rough rocky bathymetry impact waves and circulation in the nearshore. The shoreline at China Rock (Fig. 1a) and most of the bathymetry (Fig. 1b) is composed of large rocks.

Multiple datasets were combined to map the bathymetry, as in contrast to sandy shores, rocky morphology only changes on geological timescales. Multibeam bathymetry gridded at 2 m resolution for water depths greater than ≈ 10 m is available from the California State University, Monterey Bay. Shallower bathymetry was measured with a bathymetric lidar by the Joint Airborne Lidar Bathymetry Technical Center of Expertise (JALBTCX). Lidar returns have an irregular distribution, with a typical resolution between 0.5-2 m. The JALBTCX dataset covers most of the region with water depth < 10 m. Bathymetry was also measured from surveying system on a Rotinor DiveJet underwater scooter. Flotation was added to the DiveJet, which is operated at the surface by one person. A frame was mounted in front of the DiveJet to hold a survey-grade GPS above a downward-looking Nortek Signature1000 Acoustic Doppler Current Profiler (ADCP). The Nortek Signature1000 has an echosounder that was programmed to sample at 4 Hz. Subaerial topography is available from the National Oceanic and Atmospheric Administration (NOAA). Elevations relative to mean sea level (z) from the combined datasets were gridded to 2 m horizontal resolution (Fig. 1b). A local (x, y) coordinate system is defined where $-x$ is offshore directed to 285°N.

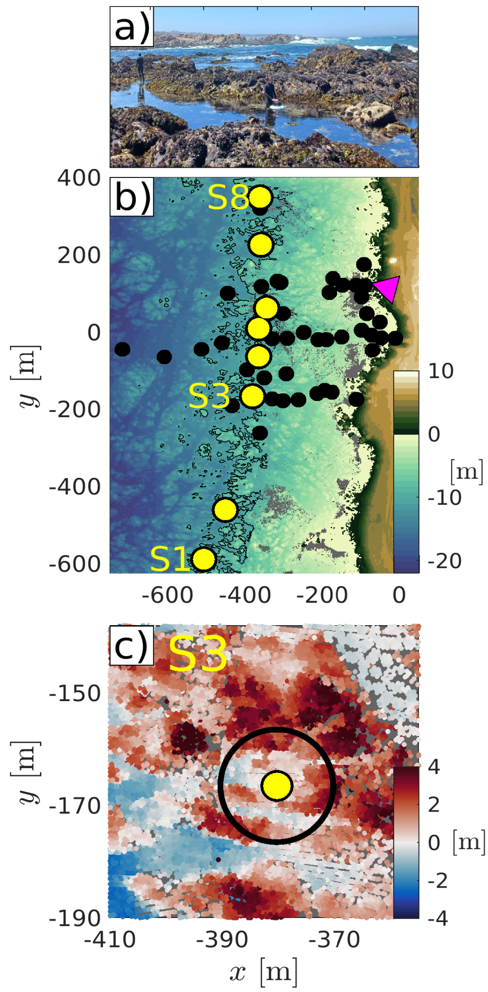

Fig. 1. (a) Image of the China Rock (Pebble Beach, CA, USA) shoreline taken at low tide, where rocks can be a few meters tall. (b) Instrument array (circles) over the rough rocky bathymetry off China Rock. An array of eight Smart Moorings (yellow dots), co-located wave buoys, and pressure sensors, was deployed at a depth of ≈ 10 m. We denote the Smart mooring locations as S1 to S8 going from south to north. Colors in (b) show the 2-m gridded elevation relative to mean sea level elevation with the 10 m isobaths contoured. Location from where the photo in (a) was taken is denoted by the magenta triangle. (c) Ungridded perturbation depth relative to the depth of the S3 pressure sensor (i.e. $-(h - \overline{h}_p)$), where positive (red) and negative (blue) indicate shallower and deeper depths than at the pressure sensor (yellow), respectively. Maps in (b) and (c) are shown in a local cross- and alongshore (x, y) coordinate system.

The shoreline and bathymetry at China Rock have variability at a wide range of scales (Fig. 1). On horizontal scales of hundreds of meters, the shoreline has small headlands and embayments spaced by 100-200 m. The bathymetry has a moderate (1:40) cross-shore slope. Rocky formations lead to large seafloor roughness on vertical scales of $O(1-10)$ m (Fig. 1c). For example, the standard deviation of z within 5 by 5 m squares has a median of 0.5 m across the study site. The difference between the maximum and minimum in each square, which is a better representation of the height of larger rocks, has a median of 2 m (consistent with the photo in Fig. 1a and the perturbation depth in Fig. 1c). In addition to areas with large bottom roughness, rock aggregates are mingled with patches of sand, where the bathymetry is smoother (e.g. around $x = -600$ m and $y = 0$ m in Fig. 1b).

b. Instruments and Data Processing

A 54-instrument array was deployed from June 17$^{\text{th}}$ to July 20$^{\text{th}}$ 2022 to measure wave transformation over the rocky bathymetry off China Rock. Instruments measuring surface gravity waves included Sofar Spotter wave buoys that measured the sea surface directly (Herbers et al. 2012; Raghukumar et al. 2019), Nortek Acoustic Doppler Current Profilers (ADCP), and bottom-mounted RBR Coda and soloD pressure sensors (blue circles in Fig. 1b). Here, we will focus on an alongshore array around the 10 m isobath of 8 Sofar Smart Moorings (yellow circles in Fig. 1), which have co-located pressure and sea-surface elevation measurements from bottom-mounted RBR Coda pressure sensors cabled to Spotter wave buoys. The Spotter provides horizontal and vertical surface displacements at frequencies 0.05 to 2.5 Hz. The co-located pressure sensors, sampling at 2 Hz, were deployed in bathymetric lows on weighted plates at a height above the local rough rocky bathymetry $z_{\text{hab}} = 0.13$ m (Fig. 1c). Given the large bottom roughness, the water depth in a pressure sensor's vicinity (i.e., at 10 m horizontal scale) can be a few meters shallower. Pressure in units of Pa is converted to units of meters by normalization with $\rho_0 g$ where $\rho_0 = 1025\ \mathrm{kg\,m^{-3}}$ and $g = 9.8\ \mathrm{m\,s^{-2}}$. Hourly-averaged atmospheric pressure P_{atm} was measured at a NOAA pressure gauge in Monterey Harbor ($\approx$ 6 km from our site). A 3 cm offset was subtracted from P_{atm} based on a comparison to our pressure sensors when exposed in the intertidal zone. The hourly-averaged water depth h_p is given by

$$h_p = \frac{P - P_{\text{atm}}}{\rho_0 g} + z_{\text{hab}}, \tag{4}$$

where P represents the hourly-averaged pressure p.

Hourly pressure spectra S_p were computed using 120 s-long segments (frequency resolution $\approx$ 0.008 Hz) that were tapered with a Hanning window and with 50% overlap yielding 118 degrees

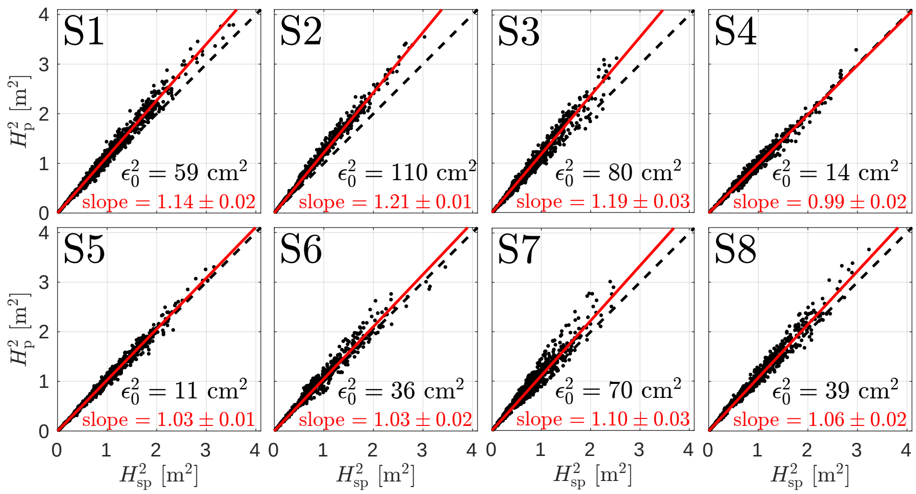

FIG. 2. Co-located pressure-based (H_p^2) versus Spotter wave-buoy-based (H_sp^2) significant wave height squared at the 8 Smart Mooring locations (Fig. 1b). The mean squared error (6) and regression slope with its 95% confidence limit are shown at each location. From the regression slopes, H_p^2 consistently overestimates H_sp^2.

of freedom. Surface elevation wave spectra S_η from the Spotter were similarly computed. The standard approach to compute S_η from S_p is to use the local depth h_p to calculate wavenumbers k through the linear dispersion relationship (3) and the transfer function K (2). This approach assumes constant depth. The significant wave height can then be computed from either Spotter (H_sp) or pressure (H_p) measurements as

$$H \equiv 4\sqrt{\int S_\eta \, \mathrm{d}f}. \tag{5}$$

Throughout this paper, we compute significant wave height H between 0.1 and 0.2 Hz. For the range in time-mean water depths at instrument locations ($9.7 < \bar{h}_p < 13.6$ m), the frequency range where H is computed corresponds to wavelengths between 36 and 105 m and kh between 0.7 and 2.2. The frequency band $0.1 < f < 0.2$ Hz includes the surface wave peak periods for most of the experiment and has negligible contamination from pressure noise amplified by K at high frequencies. Based on a S_p noise floor of 5×10^{-6} m^2 Hz^{-1} and a water depth of 13.6 m, the error in H^2 is less than 1 cm^2. In the depth range of 10–13 m, pressure-sensor-based estimates of S_η are overwhelmed by noise at frequencies higher than 0.3 Hz.

3. Accuracy of transfer function using h_p

Significant wave height H_p, estimated from pressure and the pressure-estimated local water depth h_p, is known to be accurate on low-sloped sandy coastlines (e.g., Guza and Thornton 1980), as long as kh is not too large such that sensor noise is amplified. However, the rocky bathymetry at our site has large vertical variability on horizontal scales of $O(1-10)$ m, which are shorter than the wavelength of sea and swell surface gravity waves (Fig. 1c). Thus, it is unclear whether h_p leads to reliable estimates of H_p. Since the Smart Moorings provide co-located pressure and surface elevation measurements, we can assess the accuracy H_p.

At the eight Smart Mooring locations, the Spotter significant wave height H_sp varied from 0.2 to 2 m (corresponding to a range of H_sp^2 between 0.04 and 4 m^2, Fig. 2) largely on synoptic and diurnal time scales. Here, we focus on H^2 as it directly relates to wave energy. Along the array, the time-mean H_sp^2 varied between 0.65 and 0.81 m^2, with no consistent alongshore pattern. The observed H_p^2 (using h_p) is in overall reasonable agreement with H_sp^2, but H_p^2 is biased high at most locations (Fig. 2). The accuracy of H_p^2 relative to H_sp^2 is quantified with the correlation coefficient, the linear regression slope, and the mean-squared error, i.e.

$$\epsilon_0^2 = \overline{\left(H_\mathrm{p} - H_\mathrm{sp}\right)^2}, \tag{6}$$

where $\overline{(\dots)}$ is a time average over the experiment duration (33 days), and which is proportional to the wave energy density. Both bias and random noise affect ϵ_0^2.

Along the array, H_p^2 is consistently biased high relative to H_sp^2 (Fig. 2), even though the squared correlation between the two is high at all locations ($r^2 > 0.94$, not shown). The regression slopes vary from 1.21 at S2 to 0.99 at S4 with an average of 1.09. The southernmost locations have the highest slopes. The regression slope is significantly above unity at 7 out of 8 locations, whereas the underestimate at S4 is statistically insignificant. Larger ϵ_0^2 is primarily associated with larger regression slopes (e.g., S2).

We next compare the time-average (over the experiment duration) of the Spotter wave spectra $\overline{S_\eta}$ to the pressure-sensor wave spectra $\overline{K^2(h_p)\ S_p}$ at location S3, which had a large but not the largest overestimate of H_sp^2 (Fig. 3). The mismatch between $\overline{K^2\ S_p}$ and $\overline{S}_\eta$ is frequency-dependent. In the swell band ($f < 0.1$ Hz), the two spectra are largely similar as the kh are relatively small and $K^2 \le 1.6$. However, in the sea-band ($0.1 < f < 0.2$ Hz), $\overline{K^2(h_p)\ S_p}$ is consistently elevated over $\overline{S}_\eta$, where the ratio between their sea-band integrated spectra is 1.17. Therefore, the overestimated H_p is due to sea-band waves (and not swell) as in the ≈ 10 m depth of the Smart Mooring array, the sea-band has $kh > 0.7$ corresponding to rapidly growing $K^2 = 8.3$ at $f = 0.2$ Hz. The overestimated H_p^2 and $K^2 S_p$ will lead to overestimated wave energy, wave energy fluxes, and radiation stress,

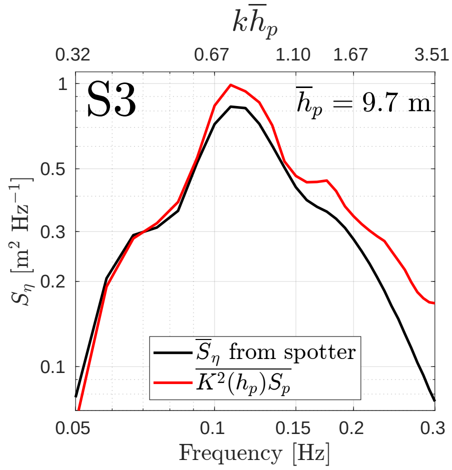

FIG. 3. Time-averaged Spotter sea-surface elevation spectra $\overline{S}_\eta$ (black) and pressure-sensor estimated $\overline{K^2 S_p}$ versus frequency at location S3. The time-averaged pressure sensor measured depth is $\bar{h}_p = 9.7$ m. The top axis shows nondimensional $k\bar{h}_p$ corresponding to the frequency axis and the $\bar{h}_p$ using the linear dispersion relationship (3).

which all depend on the sea-surface elevation spectrum. We next explore the cause of the bias between the pressure sensor and Spotter and how to correct the bias.

4. Correction of wave height estimates over complex bathymetry

The overprediction with high correlation of wave heights with pressure sensors located in bathymetric lows with dispersion relationship and transfer function evaluated at h_p, suggests that linear wave theory is largely appropriate but that using h_p leads to errors. Linear wave theory (3) and (2) is derived for a constant depth and is valid for low slopes (i.e., slowly varying bathymetry). However, here the bathymetry has large variability on horizontal scales much shorter than sea and swell wavelengths (Fig. 1c). If $K(h_p)$ was an accurate transfer function, this would suggest that surface waves would be adjusting over short horizontal distances to sharp bathymetric changes, contradicting linear theory. However, if surface gravity waves are instead only responding to water depth changes at some longer spatial scales, then simply an appropriate effective water depth h_{eff}, different than h_p is required for use in linear theory.

Our hypothesis, denoted the effective depth hypothesis, is wave statistics can be corrected by replacing h_p with an effective depth h_{eff} from the spatially smoothed bathymetry (Fig. 4). For sensors deployed in bathymetric lows, $h_{\text{eff}} < h_p$ which leads to $K(h_{\text{eff}}) < K(h_p)$ and thereby reducing the overestimation in $K^2 S_p$ and H_{p}^2. Therefore, using h_{eff} instead of h_p could reduce the observed H_{p}^2 and time-mean spectra errors. However, it is unclear a priori what the relevant

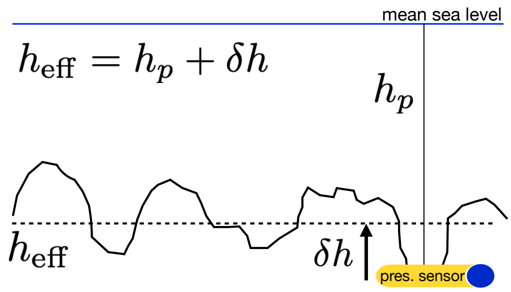

FIG. 4. Schematic of the rough bathymetry with a pressure sensor in a bathymetric low. Water depth is defined as positive, where h_p is the local depth at the pressure sensor and the effective depth h_{eff} is a spatially smoothed bathymetry. For a pressure sensor in a bathymetric low, $\delta h < 0$.

spatial scale for bathymetric-smoothing is and how to calculate a depth correction δh such that $h_{\text{eff}} = h_p + \delta h$. Using the bathymetry and co-located measurements of pressure and sea-surface elevation from the Smart Mooring array, the effective depth hypothesis can be tested. We first calculate an effective depth correction using only the wave observations and then compare it to bathymetry smoothed at different spatial scales.

a. Effective depth from observations

To determine an optimal water depth correction δh_{opt}, we find the depth correction that minimizes the error between H_{p} and H_{sp}. The error $\epsilon^2(\delta h)$ is defined similar to (6),

$$\epsilon^2(\delta h) = \overline{\left(H_{\text{p}}(h_p + \delta h) - H_{\text{sp}}\right)^2}, \tag{7}$$

where $H_{\text{p}}(h_p + \delta h)$ is based on $K^2(h_p + \delta h) S_p$ integrated between 0.1 and 0.2 Hz, and the depth change also modifies the estimated wavenumbers k in the linear dispersion relationship (3). At each location, we compute $\epsilon^2(\delta h)$ where δh is varied from -3 m to 0 m at 0.1 m intervals. The optimal water depth correction δh_{opt} equals δh that minimizes (7). Posterior estimates on the uncertainty of δh_{opt} are estimated assuming $(\epsilon^2(\delta h) - \epsilon^2(\delta h_{\text{opt}}))/\epsilon^2(\delta h_{\text{opt}})$ is a Gaussian random variable.

For example, $\epsilon^2(\delta h)$ at location S3 is shown in Fig. 5. For no depth correction ($\delta h = 0$), $\epsilon^2(\delta h)$ is equivalent to $\epsilon_0^2 = 80$ cm^2 (Fig. 2, S3). The error ϵ^2 is a parabola with δh and the optimal $\delta h_{\text{opt}} = -1.5$ m minimizes $\epsilon^2(\delta h)$ to 20 cm^2 reducing the mean squared error to one quarter of ϵ_0^2. Negative δh_{opt} is consistent with pressure sensors deployed in bathymetric lows (Fig. 1c) and the effective depth hypothesis (Fig. 4), i.e., h_{eff} is shallower than h_p. At all locations, the $\epsilon^2(\delta h)$ curve is qualitatively similar, and δh_{opt} is always negative, varying from -1.6 to -0.1 m. Note, δh_{opt} is entirely based on the pressure and wave buoy observations and does not consider the bathymetry.

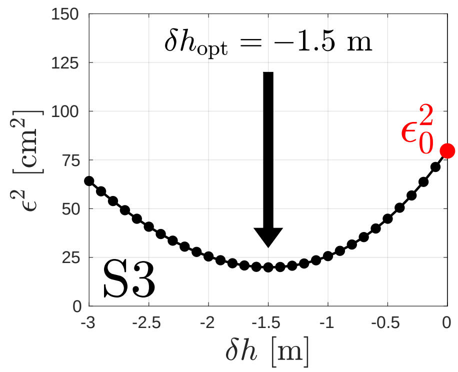

FIG. 5. Mean squared error ϵ^2 (7) between H_{p}^2 and H_{sp}^2 versus δh at location S3. The minimum of ϵ^2 gives the best correction factor (δh_{opt}).

Although we find negative optimal depth correction at all locations, δh_{opt} alone does not inform what bathymetry smoothing length scale is appropriate for computing h_{eff}.

b. Effective depth from bathymetry

Since we have the bathymetry around the Smart Mooring array, the bathymetry can be smoothed to find which length scale yields a depth correction consistent with δh_{opt}. We first quantify the rough rocky bathymetry depth statistics near the pressure sensor at S3 (Fig. 1c) from the ungridded bathymetry with its probability density function (pdf, Fig 6). Within a radius of 10 m (the nominal water depth), large depth variability occurs with max-min range of 5 m, and the 1/3 to 2/3 quantile range is 1.7 m (Fig. 6). The pressure-sensor measured time-average depth $\bar{h}_p = 9.7$ m is towards the deeper tail of the pdf, deeper than the mean and median depths of ≈ 8.9 m (a difference of 0.8 m) and consistent with the pressure sensor located in a bathymetric low.

We compute depth statistics for radii between $2 \leq r \leq 20$ m at 1 m intervals to find an appropriate horizontal smoothing scale to estimate h_{eff}. At every r, the depth correction is given by

$$\delta h(r) \equiv [h](r) - \bar{h}_p, \tag{8}$$

where $[h](r)$ is either the mean or median water depth within a distance r from the pressure sensor (e.g. circle with $r = 10$ m is shown in Fig. 1c). In general, each location has an optimal smoothing scale resulting in a r and a δh that matches δh_{opt}. For a simple depth correction that can be applied to any sensor, a single length scale was determined by minimizing the depth correction error, i.e.,

$$\mathcal{E}^2(r) = \langle \left(\delta h(r) - \delta h_{\mathrm{opt}}\right)^2 \rangle, \tag{9}$$

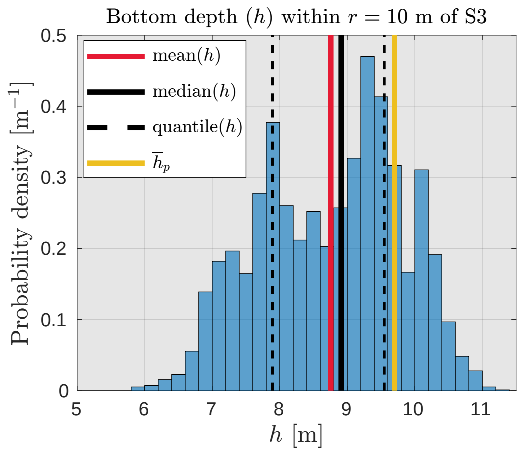

Fig. 6. Probability density function of water depths h within a circul with radius r = 10 m (circle in Fig. 1c) centered on the pressure sensor location. The bathymetry statistics mean depth (red), median depth (solid black), 1/3 and the 2/3 quantiles (dashed black lines) are shown as is the time-mean pressure sensor estimated depth $\bar{h}_p$ (yellow).

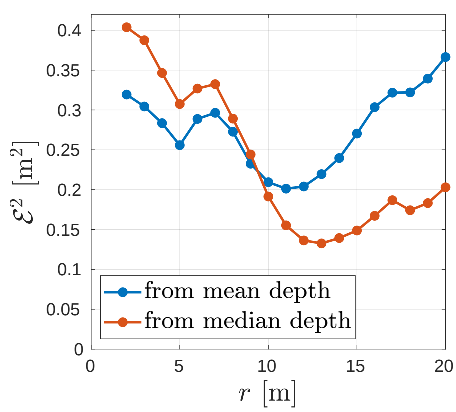

Fig. 7. Average bathymetric correction error $\mathcal{E}^2$ (9) versus r based on mean (blue) and median (orange) water depths.

where $\langle\cdot\rangle$ is an average across eight locations. The minimum of $\mathcal{E}^2$ gives the optimal smoothing horizontal length scale $\hat{r}$ and we define $\delta h_{\text{bathy}} \equiv \delta h(\hat{r})$.

The mean squared errors $\mathcal{E}^2$ have well-defined global minima at $\hat{r} = 11$ m for the mean and $\hat{r} = 13$ m for the median (Fig. 7). The median at $\hat{r} = 13$ m has $\mathcal{E}^2$ that is 25% reduced from the mean at $\hat{r} = 11$ m, suggesting that the median bathymetry at $\hat{r} = 13$ m is the appropriate smoothing scale at this water depth. We calculate δh_{bathy} at all locations using the median bathymetry at $\hat{r} = 13$ m. As expected, all locations have $\delta h_{\text{bathy}} < 0$, indicating that pressure sensors were in relative bathymetric lows. Five locations (S1, S2, S3, S7, S8) had rougher bathymetry and deeper bathymetric lows $-1.5 \le \delta h_{\mathrm{bathy}} \le -1$ m, whereas $\delta h_{\mathrm{bathy}} > -0.7$ m indicates a smoother bottom at the other three locations (S4, S5, S6).

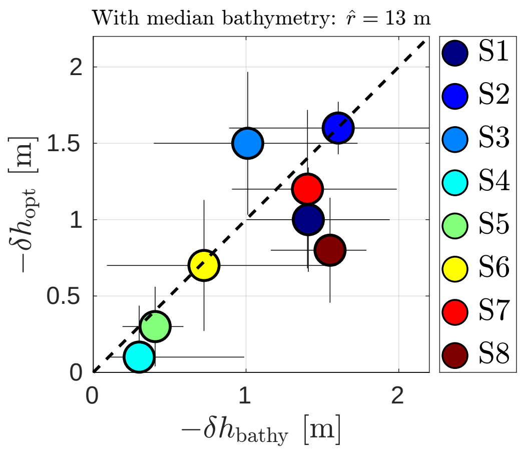

Fig. 8. Optimal depth correction $-\delta h_{\mathrm{opt}}$ versus smoothed bathymetry depth correction $-\delta h_{\mathrm{bathy}}$ using median depth with $\hat{r} = 13$ m. The dashed line represents the 1-to-1 line. The horizontal bars represent the 1/3 to 2/3 bathymetry quantile range. The vertical error bars represent the uncertainty in the δh_{opt} estimate.

c. Accuracy of transfer function at h_{eff}

The bathymetric corrections $\delta h_{\mathrm{bathy}}$ using a single smoothing scale $\hat{r} = 13$ m are consistent with δh_{opt} (Fig. 8). In terms of magnitude, the corrections qualitatively have two groupings. The first grouping (S4, S5, S6) has smaller (≤ 0.7 m) depth corrections $\delta h_{\mathrm{bathy}}$, whereas the second grouping (S1, S2, S3, S7, S8) has larger 1–1.5 m corrections (Fig. 8). These two groupings are separated by the δh_{opt} error bars and the 1/3-2/3 bathymetric quantiles (vertical and horizontal bars in Fig. 8). The $\delta h_{\mathrm{bathy}}$ is roughly proportional to δh_{opt} with a near-one slope. Location S8 has the largest deviation from the one-to-one line with a 0.8 m difference between δh_{opt} and $\delta h_{\mathrm{bathy}}$. The overall similarity between δh_{opt} and $\delta h_{\mathrm{bathy}}$ supports the effective depth hypothesis.

We next explore how using a h_{eff} derived from either δh_{opt} or $\delta h_{\mathrm{bathy}}$ improves the significant wave height estimates at location S3 (Fig. 9), a site with relatively large $\delta h_{\mathrm{opt}} = -1.5$ m and $\delta h_{\mathrm{bathy}} = -1$ m. As in Fig. 2, the uncorrected H_{p}^2 leads to large errors $\epsilon_0^2 = 80$ cm^2 and a large regression slope of 1.19 (Fig. 9a). With the optimal correction $h_{\mathrm{eff}} = h_p + \delta h_{\mathrm{opt}}$, H_{p}^2 more closely matches H_{sp}^2 (Fig. 9b) with best-fit slope near one and small $\epsilon^2 = 20$ cm^2. With the bathymetric correction $h_{\mathrm{eff}} = h_p + \delta h_{\mathrm{bathy}}$, H_{p}^2 is also much closer to H_{sp}^2 than for the uncorrected. The error $\epsilon^2 = 26$ cm^2, is slightly elevated from that of δh_{opt} and reduced nearly 70% relative to the uncorrected. The best-fit slope is 1.08, indicating a nearly 60% reduction in the bias.

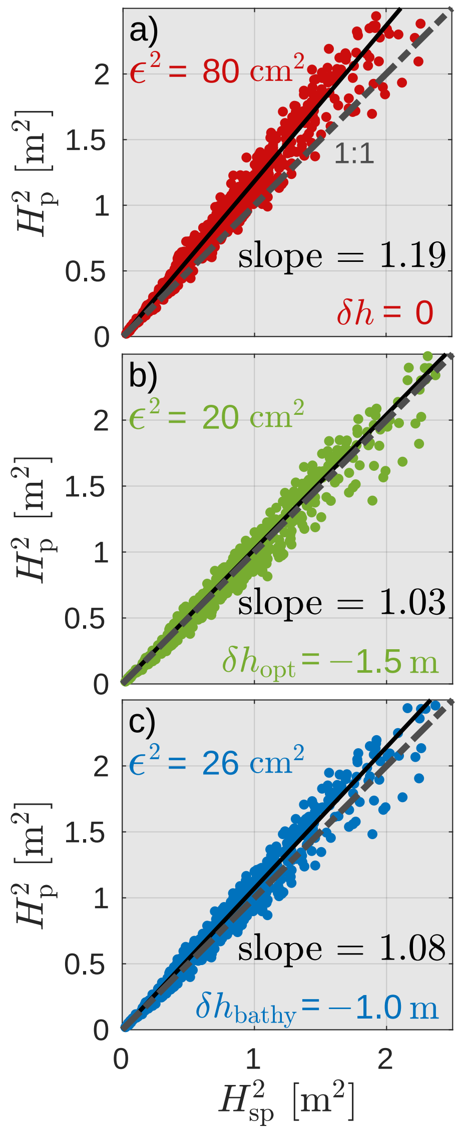

FIG. 9. H_{p}^2 versus H_{sp}^2 at location S3, where the transfer function is computed at (a) $\bar{h}_p$, (b) $h_{\mathrm{eff}} = \bar{h}_p + \delta h_{\mathrm{opt}}$, or (c) $h_{\mathrm{eff}} = \bar{h}_p + \delta h_{\mathrm{bathy}}$. The bathymetric correction δh, the mean squared error (7), and the linear regression slope are shown in each panel.

Using either the optimal or bathymetrically-smoothed h_{eff} ($< h_p$) reduces H_{p}^2 to be closer to H_{sp}^2. We next examine the effect of the two depth corrections in frequency space using the time-averaged wave spectra S_η at S3 (Fig. 10). As in Fig. 3, the uncorrected $\overline{K^2(h_p)\ S_p}$ overpredicts the Spotter $\overline{S_\eta}$ for $0.1 < f < 0.2$ Hz (or $0.67 < k\bar{h}_p < 1.67$, black curve Fig. 10), with ratio between their sea-band integrated spectra of 1.17. With $\delta h_{\mathrm{opt}} = -1.5$ m, the spectra $\overline{K^2(h_p + \delta h_{\mathrm{opt}})\ S_p}$ is similar to the Spotter $\overline{S_\eta}$ across the $0.1 < f < 0.2$ Hz band (green curve, Fig. 10) with ratio of their integrated spectra of 1.00, consistent with the changes in best-fit slope (Fig. 9b). The difference between

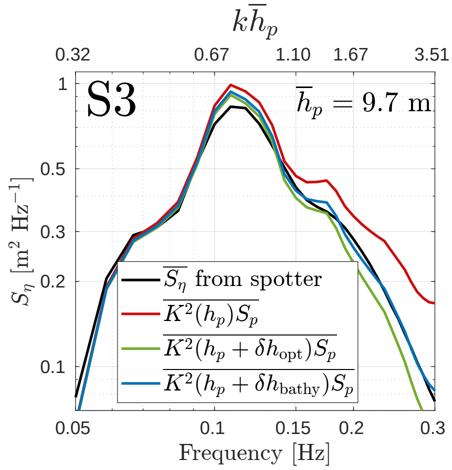

FIG. 10. Time-averaged surface elevation spectra versus frequency at location S3. Similar to Fig. 3, the black-curve is Spotter-estimated $\overline{S}_\eta$. Three pressure-sensor estimated spectra are shown: for no depth correction (red, $\overline{K^2(h_p)S_p}$), optimal depth correction (green, $\overline{K^2(h_p+\delta h_{\mathrm{opt}})S_p}$), and smoothed bathymetric correction (blue, $\overline{K^2(h_p+\delta h_{\mathrm{bathy}})S_p}$). The top axis shows the corresponding nondimensional $k\bar{h}_p$ where $\bar{h}_p = 9.7$ m.

$\overline{K^2(h_p+\delta h_{\mathrm{opt}})\;S_p}$ and the uncorrected $\overline{K^2(h_p)\;S_p}$ is small near $f = 0.1$ Hz and increases with f (or kh). Even out to $f = 0.3$ Hz, $\overline{K^2(h_p+\delta h_{\mathrm{opt}})\;S_p}$ is much closer to $\overline{S_\eta}$ than $\overline{K^2(h_p)\;S_p}$, indicating the correction using δh_{opt} performs well beyond the frequency-band considered for significant wave height. With $\delta h_{\mathrm{bathy}} = -1$ m, the spectra $\overline{K^2(h_p+\delta h_{\mathrm{bathy}})\;S_p}$ is also similar to the Spotter $\overline{S_\eta}$ for $0.1 < f < 0.2$ Hz (blue curve, Fig. 10) with ratio of their sea-band integrated spectra of 1.05, also consistent with the changes in best-fit slope (Fig. 9c). At lower frequencies $f < 0.1$ Hz, the spectra using h_p or the optimal or bathymetric depth corrections result in similar time-mean spectra as kh is relatively small (< 0.66), resulting in small changes to K^2.

We next examine the significant wave height errors using the uncorrected ($\delta h = 0$), optimal ($\delta h = \delta h_{\mathrm{opt}}$), and smoothed bathymetry using $\hat{r} = 13$ m ($\delta h = \delta h_{\mathrm{bathy}}$) across all eight locations (Fig. 11). As seen in Fig. 2, the uncorrected error $\epsilon_0^2 = \epsilon^2(0)$ varies by factor of 10, from 110 at S2 to 11 cm^2 at S5 (red bars in Fig 11). The error with optimal correction $\epsilon^2(\delta h_{\mathrm{opt}})$ (green bars in Fig 11) is reduced substantially ($> 50\%$) relative to ϵ_0^2 at locations with significant ϵ_0^2, such as the S1, S2, S3, S7, and S8 grouping. At locations with weak ϵ_0^2 (S4 and S5), the optimal correction δh_{opt} is small and results in $\epsilon^2(\delta h_{\mathrm{opt}})$ are similar to ϵ_0^2. At all locations but S8, the smoothed bathymetry correction $\epsilon^2(\delta h_{\mathrm{bathy}})$ (blue bar, Fig. 11) is similar to $\epsilon^2(\delta h_{\mathrm{opt}})$, indicating that using the depth from the smoothed bathymetry enables accurate estimation of wave statistics. Location S8 is an outlier, as $\epsilon^2(\delta h_{\mathrm{bathy}})$ is only slightly reduced from ϵ_0^2. This location also had the largest deviation between δh_{opt} and $\delta h_{\mathrm{bathy}}$ (dark red in Fig. 8). It is unclear why this location is an outlier.

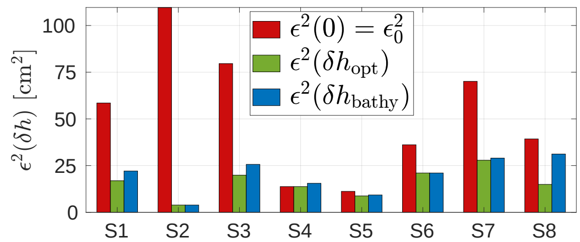

FIG. 11. Mean squared error of H_p^2 relative to H_{sp}^2 (7) using local depth ($\delta h = 0$, red), the optimal depth correction (δh_{opt}, green) and the correction from the median bathymetry at $\hat{r} = 13$ m (δh_{bathy}, blue).

5. Discussion

For pressure sensors deployed in bathymetric lows, using linear theory with h_p gives rise to clear errors in significant wave height H_p^2 and wave spectra. The agreement between δh_{opt} and δh_{bathy} and the error reduction between ϵ_0^2 and $\epsilon^2(\delta h_{bathy})$ strongly supports the effective depth hypothesis that a water depth based on a spatially averaged bathymetry is the appropriate depth to use in linear theory on rough rocky bathymetry with large variability on small spatial scales. We next examine the errors between pressure- and Spotter-based wave statistics relative to a sandy, smooth inner-shelf, discuss the implications of an effective depth, and application to other regions.

a. Comparison to a smooth, sandy inner-shelf

Comparisons between co-located pressure sensors and Spotter wave buoys on the inner-shelf are not common. In a low-sloped sandy bay in $h \approx 7$ m depth, a pressure sensor integrated within an ADCP (Acoustic Doppler Current Profiler) had good time-mean sea-surface spectra comparison in the sea-swell band to a Spotter wave buoy (Lancaster et al. 2021). More recently, a range of wave buoys were intercompared to a pressure sensor array in 8-m water depth on a low sloped and smooth sandy beach (Collins et al. 2023). The Spotter was deployed 400 m alongshore from the pressure sensor array over 3 winter months and the observed H_{sp}varied from 0.5-3 m, generally larger than observed here (Fig. 2). In a 0.1-Hz wide band spanning similar kh ranges as here, the Collins et al. (2023) ϵ_0 (6) is 36 cm^2, which is partially attributable to process noise (e.g., true alongshore variations in wave height) as the sensors were not co-located. Taking into account processes noise and the larger H_{sp}, the Collins et al. (2023) $\epsilon_0 = 36$ cm^2 is consistent with the smaller ϵ observed here at locations (S4, S5, S6, and S8) all of which except S8, had small δh_{opt} and δh_{bathy} (Fig. 8). The locations with ϵ_0 much larger than that of Collins et al. (2023) (i.e., S1, S2, S3, S7) had large δh_{opt} and δh_{bathy} (with magnitudes > 1 m), and the corrections significantly improved the errors. The elevated mean-square-error in wave statistics for pressure sensors deployed in bathymetric lows, particularly relative to smooth sandy inner shelf, demonstrates the need for correcting pressure-sensor based wave statistics on rough rocky bathymetries.

b. Implications of an effective depth

On larger scales, the ROXSI bathymetric slope is weak ≈ 0.025. However, the rough rocky bathymetry has large variability, with bottom slopes greater than 0.52 (30°), over short horizontal scales of $O(1)$ m (Fig. 1). Even with this small-scale bathymetric variability, surface gravity waves propagate coherently over rough rocky bathymetry as if there is a dispersion relationship with an effective depth that is some spatial average of the bathymetry they are propagating over. For pressure sensors in bathymetric lows in 10–13 m water depth, we found a smoothing length scale of $\hat{r} = 13$ m led to the largest reduction in error in the 0.1–0.2 Hz band. Therefore, high-resolution bathymetry mapping is required to calculate the effective depth. However, even with such detailed knowledge of the bathymetry, for locations in other water depths or other frequencies, the appropriate smoothing scale is unclear. Via dimensional reasoning, we argue that the relevant nondimensional parameter is the ratio of the smoothing scale to the wavelength $\hat{r}/\lambda$. One could imagine that each frequency would have its own associated smoothing scale, but here we focus on a single frequency. The largest spectra corrections are near 0.2 Hz corresponding to $k\bar{h}_p = 1.67$ (Fig. 10), with corresponding wavelength $\lambda \approx 37$ m (with $\bar{h}_p \approx 10$ m), resulting in a ratio $\hat{r}/\lambda \approx 1/3$. This may provide guidance for correcting pressure-sensor based wave statistics in other water depths given the same $kh = 1.67$ cutoff.

The fluid dynamics of orbital velocities and pressure near the bottom of rough rocky bathymetry is largely unstudied. Our results imply that the bed is effectively at $z = -h_{\text{eff}}$ for the dispersion relationship (3) and the transfer function (2) and that the wave pressure signal does not decay in the vertical for $-h_p \leq z \leq -h_{\text{eff}}$. We hypothesize that the constant pressure below $z = -h_{\text{eff}}$ is because horizontal orbital velocities, which vary on horizontal scales of λ, are largely constrained to be zero within bathymetric lows that have much shorter horizontal length scales (e.g., Fig. 1c). This implies a spatially uniform but time-varying velocity potential below $z = -h_{\text{eff}}$, which, through Bernoulli's equation, leads to a spatially uniform and time varying wave-induced pressure. Further work on detailed near-bottom wave dynamics over rough rocky bathymetry is forthcoming.

c. Application to coral reefs

The errors in pressure-based wave measurements observed on rough rocky bathymetry may also occur in other regions with large bathymetric roughness such as coral reefs. Previous work have not addressed the accuracy of flat-bottom linear wave theory applied to coral reef pressure measurements. For known root-mean-squared bottom depth variability (σ_b) in the vicinity of a pressure sensor, the ratio $\cosh^2(kh_p)/\cosh^2(k(h_p-\sigma_b))$ provides a rough magnitude estimate of the potential overestimate in wave energy density at a single frequency from a near-bottom pressure sensor in a bathymetric low. For small kh_p, the ratio is ≈ 1 and errors are negligible. Errors grow with kh_p. Waves observed on shallow reef flats with $h \approx 1$ m and $\sigma_b = 15$ cm and peak periods from 4–8 s, result in a 4% overestimate at 4 s (Lentz et al. 2016). Similar reef flat observations with 10 s peak periods lead to no error (Sous et al. 2023). In deeper water reef observations ≈ 7 m, errors in wave statistics are potentially larger, although the roughness in this depth was not reported (Lowe et al. 2005). Over the rougher coral reefs at the Palmyra atoll, with $0.4 \leq \sigma_b \leq 1.3$ m, observations at $h \approx 11$ m may be as accurate as 2% for low-frequency swell, but overestimates can be as large 15% for 7-s seas (Monismith et al. 2015; Rogers et al. 2016). Larger depth changes over spur-and-groove formations in coral reefs can imply biases of up to 35% from pressure sensors in 2-m deep grooves in water depths of 10 m for mean wave period of 6 s (Acevedo-Ramirez et al. 2021). This suggests that analogous errors may be present in some pressure-sensor based wave statistics on coral reefs.

6. Summary

We present surface gravity wave observations from eight co-located bottom-mounted pressure sensors and Spotter wave buoys in 10–13 m water depth from the five-week ROXSI field experiment, at a site with rough rocky bathymetry on the Monterey Peninsula. The rough bathymetry has large $O(1)$ m vertical variability on $O(1-10)$ m horizontal scales. Pressure sensors were deployed by divers in rocky bathymetric lows to enhance sensor stability in large waves. Using the pressure-sensor estimated water depth h_p, the pressure-based significant wave height squared consistently overestimates (as large as 21%) wave buoy measurements. Some locations have large mean square error (ϵ_0^2) between pressure- and buoy-based wave height, far larger than analogous measurements on a sandy, low-sloped inner-shelf. The time-mean pressure-sensor based wave spectra are elevated in sea-band (0.1-0.2 Hz) relative to the Spotter. These errors are consistent with the depth h_p used in the linear-theory based transformation being too large. An effective depth hypothesis is proposed, where a depth based on a spatially smoothed bathymetry is the appropriate depth to use with linear theory for estimating wave statistics from pressure observations. An optimal depth correction δh_{opt} is estimated by minimizing the error between significant wave heights from pressure sensors and Spotter wave buoys. The optimal correction to the local depth is $-1.6 \leq \delta h_{\mathrm{opt}} < -0.1$ m across the eight locations, where the sign is consistent with pressure sensors in bathymetric lows and an effective depth shallower than h_p. A bathymetry smoothing scale of $\hat{r} = 13$ m (or 1/3 of wavelength of 0.2 Hz waves in 10-m depth) is found by minimizing the squared difference between the smoothed bathymetry correction and the optimal bathymetry correction. The optimal and smoothed-bathymetric depth corrections are similar across locations. Both corrections, using linear theory, significantly improve errors in wave statistics, particularly in locations with large δh_{bathy} and large errors ϵ_0^2. This indicates that the effective depth hypothesis is valid and that a depth based on spatially averaged bathymetry is the appropriate depth to use in linear theory on rough rocky bathymetry. For application in other depths or frequencies, we argue that the smoothing length scale should be $\approx 1/3$ of the wavelength of the higher frequency waves of interest. Similar errors to those seen here may also be present in pressure-based wave statistics on rough coral reefs.

Acknowledgments. This paper is part of the ROcky Shore: eXperiment and SImulations (ROXSI) project, funded by the Office of Naval Research through grants N000142112786 and N0001423WX01357. The Monterey NOAA Sanctuary, CA Fish and Wildlife, Pebble Beach, and Pacific Grove provided environmental permission for the experiment with permitting support provided by Chris Miller. We thank the SIO and NPS field crews for their invaluable support with the field experiment; for SIO: Brian Woodward, Kent Smith, Rob Grenzeback, Lucian Parry, Shane Finnerty, Carson Black, Duncan Wheeler, Annie Adelson, Loren Clark, Kaden Quinn, and Kanoa Pick; for NPS: Paul Jessen, Charlotte Benbow, Pat Collins, Mike Cook, Matt Gough, and Ian Jenstrom. We appreciate the valuable discussions with the ROXSI team (Johanna Rosman, Greg Wilson, Ata Suanda, Mika Malila, Matt Conlin, César Acevedo-Ramirez) that informed this manuscript.

Data availability statement. The data presented in this paper will be made freely available upon publication.

References

Acevedo-Ramirez, C. A., W. Stephenson, S. Wakes, and I. Mariño-Tapia, 2021: Wave transformation on a fringing reef system with spur and groove structures. *Journal of Geophysical Research: Oceans*, **126 (9)**, e2020JC016 910, https://doi.org/10.1029/2020JC016910.

Bertin, X., and Coauthors, 2018: Infragravity waves: From driving mechanisms to impacts. *Earth-Science Reviews*, **177**, 774–799, https://doi.org/10.1016/j.earscirev.2018.01.002.

Bishop, C., and M. Donelan, 1987: Measuring waves with pressure transducers. *Coastal Engineering*, **11 (4)**, 309–328, https://doi.org/10.1016/0378-3839(87)90031-7.

Bonneton, P., and D. Lannes, 2017: Recovering water wave elevation from pressure measurements. *Journal of Fluid Mechanics*, **833**, 399–429, https://doi.org/10.1017/jfm.2017.666.

Bonneton, P., D. Lannes, K. Martins, and H. Michallet, 2018: A nonlinear weakly dispersive method for recovering the elevation of irrotational surface waves from pressure measurements. *Coastal Engineering*, **138**, 1–8, https://doi.org/10.1016/j.coastaleng.2018.04.005.

Collins, C. O., P. Dickhudt, J. Thomson, E. Terrill, and L. Centurioni, 2023: Performance of moored gps wave buoys. *Coastal Engineering Journal*, submitted.

Davis, K. A., G. Pawlak, and S. G. Monismith, 2021: Turbulence and coral reefs. *Annual Review of Marine Science*, **13**, 343–373, https://doi.org/10.1146/annurev-marine-042120-071823.

Dean, R. G., and R. A. Dalrymple, 1991: *Water Wave Mechanics for Engineers and Scientists*, Vol. 2. World Scientific Publishing Company.

Elfrink, B., and T. Baldock, 2002: Hydrodynamics and sediment transport in the swash zone: a review and perspectives. *Coastal Engineering*, **45 (3-4)**, 149–167, https://doi.org/10.1016/S0378-3839(02)00032-7.

Elgar, S., B. Raubenheimer, and R. Guza, 2001: Current meter performance in the surf zone. *Journal of Atmospheric and Oceanic Technology*, **18 (10)**, 1735–1746, https://doi.org/10.1175/1520-0426(2001)018⟨1735:CMPITS⟩2.0.CO;2.

Farrell, E. J., H. Granja, L. Cappietti, J. T. Ellis, B. Li, and D. J. Sherman, 2009: Wave transformation across a rock platform, belinho, portugal. *Journal of Coastal Research*, **(1, 56)**, 44–48, 10th International Coastal Symposium (ICS 2009), Lisbon, PORTUGAL, APR 13-18, 2009.

Gomes da Silva, P., G. Coco, R. Garnier, and A. H. F. Klein, 2020: On the prediction of runup, setup and swash on beaches. *Earth-Science Reviews*, **204**, https://doi.org/10.1016/j.earscirev.2020.103148.

Gon, C. J., J. H. MacMahan, E. B. Thornton, and M. Denny, 2020: Wave dissipation by bottom friction on the inner shelf of a rocky shore. *Journal of Geophysical Research: Oceans*, **125 (10)**, https://doi.org/10.1029/2019JC015963.

Guza, R., and E. B. Thornton, 1980: Local and shoaled comparisons of sea surface elevations, pressures, and velocities. *Journal of Geophysical Research: Oceans*, **85 (C3)**, 1524–1530, https://doi.org/https://doi.org/10.1029/JC085iC03p01524.

Hasselmann, K., 1962: On the non-linear energy transfer in a gravity-wave spectrum part 1. general theory. *Journal of Fluid Mechanics*, **12 (4)**, 481–500, https://doi.org/10.1017/S0022112062000373.

Herbers, T., S. Elgar, and R. Guza, 1999: Directional spreading of waves in the nearshore. *Journal of Geophysical Research: Oceans*, **104 (C4)**, 7683–7693, https://doi.org/https://doi.org/10.1029/1998JC900092, URL https://agupubs.onlinelibrary.wiley.com/doi/abs/10.1029/1998JC900092.

Herbers, T., S. Elgar, N. Sarap, and R. Guza, 2002: Nonlinear dispersion of surface gravity waves in shallow water. *Journal of Physical Oceanography*, **32 (4)**, 1181–1193, https://doi.org/10.1175/1520-0485(2002)032⟨1181:NDOSGW⟩2.0.CO;2.

Herbers, T., R. Lowe, and R. Guza, 1992: Field observations of orbital velocities and pressure in weakly nonlinear surface gravity waves. *Journal of Fluid Mechanics*, **245**, 413–435, https://doi.org/10.1017/S0022112092000521.

Herbers, T. H. C., P. F. Jessen, T. T. Janssen, D. B. Colbert, and J. H. MacMahan, 2012: Observing ocean surface waves with gps-tracked buoys. *Journal of Atmospheric and Oceanic Technology*, **29 (7)**, 944 – 959, https://doi.org/https://doi.org/10.1175/JTECH-D-11-00128.1.

Lancaster, O., R. Cossu, S. Boulay, S. Hunter, and T. E. Baldock, 2021: Comparative wave measurements at a wave energy site with a recently developed low-cost wave buoy (spotter), adcp, and pressure loggers. *Journal of Atmospheric and Oceanic Technology*, **38 (5)**, 1019–1033, https://doi.org/10.1175/JTECH-D-20-0168.1.

Lavaud, L., X. Bertin, K. Martins, M. Pezerat, T. Coulombier, and D. Dausse, 2022: Wave dissipation and mean circulation on a shore platform under storm wave conditions. *Journal of Geophysical Research: Earth surface*, **127 (3)**, https://doi.org/10.1029/2021JF006466.

Lentz, S., and B. Raubenheimer, 1999: Field observations of wave setup. *Journal of Geophysical Research: Oceans*, **104 (C11)**, 25 867–25 875, https://doi.org/https://doi.org/10.1029/1999JC900239.

Lentz, S. J., J. H. Churchill, K. A. Davis, and J. T. Farrar, 2016: Surface gravity wave transformation across a platform coral reef in the red sea. *Journal of Geophysical Research: Oceans*, **121 (1)**, 693–705, https://doi.org/10.1002/2015JC011142.

Lowe, R., J. Falter, M. Bandet, G. Pawlak, M. Atkinson, S. Monismith, and J. Koseff, 2005: Spectral wave dissipation over a barrier reef. *Journal of Geophysical Research: Oceans*, **110 (C4)**, https://doi.org/10.1029/2004JC002711.

MacMahan, J., E. Thornton, and A. Reniers, 2006: Rip current review. *Coastal Engineering*, **53 (2-3, SI)**, 191–208, https://doi.org/10.1016/j.coastaleng.2005.10.009, international Symposium on Coastal Hydrodynamics and Morphodynamics, Delft Univ Technol, Delft, NETHERLANDS, MAR 13-14, 2004.

Martins, K., P. Bonneton, D. Lannes, and H. Michallet, 2021: Relation between orbital velocities, pressure, and surface elevation in nonlinear nearshore water waves. *Journal of Physical Oceanography*, **51 (11)**, 3539–3556, https://doi.org/10.1175/JPO-D-21-0061.1.

Monismith, S. G., 2007: Hydrodynamics of coral reefs. *Annual Review of Fluid Mechanics*, **39**, 37–55, https://doi.org/10.1146/annurev.fluid.38.050304.092125.

Monismith, S. G., J. S. Rogers, D. Koweek, and R. B. Dunbar, 2015: Frictional wave dissipation on a remarkably rough reef. *Geophysical Research Letters*, **42 (10)**, 4063–4071, https://doi.org/10.1002/2015GL063804.

Moulton, M., S. H. Suanda, J. C. Garwood, N. Kumar, M. R. Fewings, and J. M. Pringle, 2023: Exchange of plankton, pollutants, and particles across the nearshore region. *Annual Review of Marine Science*, **15**, 167–202, https://doi.org/10.1146/annurev-marine-032122-115057.

Poate, T., G. Masselink, M. J. Austin, M. Dickson, and R. McCall, 2018: The role of bed roughness in wave transformation across sloping rock shore platforms. *Journal of Geophysical Research: Earth Surface*, **123 (1)**, 97–123, https://doi.org/10.1002/2017JF004277.

Raghukumar, K., G. Chang, F. Spada, C. Jones, T. Janssen, and A. Gans, 2019: Performance characteristics of “spotter,” a newly developed real-time wave measurement buoy. *Journal of Atmospheric and Oceanic Technology*, **36 (6)**, 1127 – 1141, https://doi.org/10.1175/JTECH-D-18-0151.1.

Raubenheimer, B., R. Guza, and S. Elgar, 1996: Wave transformation across the inner surf zone. *Journal of Geophysical Research: Oceans*, **101 (C11)**, 25 589–25 597, https://doi.org/https://doi.org/10.1029/96JC02433.

Raubenheimer, B., R. T. Guza, and S. Elgar, 2001: Field observations of wave-driven setdown and setup. *Journal of Geophysical Research: Oceans*, **106 (C3)**, 4629–4638, https://doi.org/https://doi.org/10.1029/2000JC000572.

Rogers, J. S., S. G. Monismith, D. A. Koweek, and R. B. Dunbar, 2016: Wave dynamics of a pacific atoll with high frictional effects. *Journal of Geophysical Research: Oceans*, **121 (1)**, 350–367, https://doi.org/10.1002/2015JC011170.

Sous, D., K. Martins, M. Tissier, F. Bouchette, and S. Meule, 2023: Spectral wave dissipation over a roughness-varying barrier reef. *Geophysical Research Letters*, **50 (5)**, https://doi.org/10.1029/2022GL102104.

Thornton, E., and R. Guza, 1982: Energy saturation and phase speeds measured on a natural beach. *Journal of Geophysical Research: Oceans*, **87 (NC12)**, 9499–9508, https://doi.org/10.1029/JC087iC12p09499.

Thornton, E., and R. Guza, 1983: Transformation of wave height distribution. *Journal of Geophysical Research: Oceans*, **88 (NC10)**, 5925–5938, https://doi.org/10.1029/JC088iC10p05925.